Contract No.:

This manuscript has been authored by Savannah River Nuclear Solutions (SRNS), LLC under Contract No. DE-AC09-08SR22470 with the U.S. Department of Energy (DOE) Office of Environmental Management (EM).

Hydrogen desorption using honeycomb finned heat exchangers integrated in adsorbent storage systems

Claudio Corgnale[1,2], Bruce Hardy[1*], Richard Chahine[3], Daniel Cossement[3]
1 Savannah River National Laboratory, Aiken, SC 29808, USA
2 Greenway Energy, Aiken, SC 29803, USA
3 Hydrogen Research Institute, Université du Québec à Trois-Rivières, Trois-Rivières, QC, Canada. G9A 5H7

ABSTRACT

One of the main technical hurdles associated with adsorbent based hydrogen storage systems is relative to their ability to discharge hydrogen effectively, as dictated by fuel cell requirements. A new honeycomb finned heat exchanger concept was examined to evaluate its potential as a heat transfer system for hydrogen desorption. A bench scale 0.5 L vessel was equipped with the proposed heat exchanger, filled with MOF-5® adsorbent material. The heating power, required to desorb hydrogen, was provided by a 100 W electric heater placed in the center of the honeycomb structure. Two desorption tests, at room temperature and under cryogenic temperatures, were carried out to evaluate the hydrogen desorption performance of the proposed system under different operating conditions. The bench scale vessel performance was verified from both an experimental and a modeling point of view, demonstrating the ability to desorb about 45% of the adsorbed hydrogen in reduced time and applying low heating power. Further modeling analyses were also carried out showing the potential of the proposed system to reach high hydrogen discharging rates at cryogenic temperature conditions and operating pressures between 100 bar and 5 bar. The proposed adsorption system also demonstrated to be able to discharge all the available hydrogen in less than 500 s operating at cryogenic conditions and with a nominal heating power of 100 W.

Nomenclature

c =	Molar concentration of H_2 (mol/m^3)
$C_{P\,Ads}$ =	Specific heat of adsorbent (J/kg-K)
E_a =	Characteristic free energy of adsorption from the Dubinin-Astakhov model (J/mol). $\equiv \alpha+\beta T$
h =	Molar enthalpy of the gas (J/mol)
$\underline{\underline{I}}$ =	2nd order identity tensor
k =	Thermal conductivity (W/(m-K))
M_{H2} =	Molecular weight of hydrogen (0.002016 kg/g-mol)
n_a =	Absolute adsorption (mol of H_2/kg of adsorbent)

* Corresponding author email: bruce.hardy@srnl.doe.gov.

n_{ex} = Adsorbed hydrogen excess, compared to gaseous state hydrogen (mol of H_2/kg of adsorbent)

n_{max} = Limiting adsorption, associated with the maximum hydrogen loading of the entire adsorption volume (mol of H_2/(kg of adsorbent))

n_{total} = Total hydrogen stored in the bed (mol of H_2/(kg of adsorbent))

P = Pressure (Pa)

P_0 = Pseudo-pressure for Dubinin-Astakhov model (Pa)

R = Gas constant = 8.314 J/(mol-K)

S_0 = Mass source of hydrogen per unit of total volume (kg/m^3-s)

T = Temperature (K)

t_w = Hexagonal cell wall thickness (m)

u_0= Molar internal energy of free gas at the system temperature T and a pressure of 1 atm (J/mol)

V_a = Adsorbed volume per mass of adsorbent (m^3/(kg of adsorbent)). The void volume within the adsorbent for which the gas concentration exceeds that given by the equation of state, per mass of adsorbent.

Vadsorbent = Volume occupied by the adsorbent material (m^3)

V_v = Void volume per mass of adsorbent (m^3/(kg of adsorbent)), measured by He filling.

$\vec{v}$ = Mean interstitial gas velocity vector (m/s) or velocity of gas (m/s)

$\vec{v}_s$ = Superficial velocity vector (m/s)

W_a = Adsorption/Desorption heat related power (W/m^3)

W_c = Hexagonal cell width, flat to flat side (m)

W_p = Compression/Expansion work related power (W/m^3)

Z = Hydrogen compressibility factor.

Greek

α = Enthalpic contribution to the characteristic free energy of adsorption, E_a, (J/mol)

β = Entropic contribution to the characteristic free energy of adsorption, E_a, (J/mol-K)

ε = Effective porosity, volume available for flow = ρ_{Carbon} (V_v-V_a)

ΔU_a = Internal energy per mass of adsorbent of the condensed phase of the gas at a temperature T and pressure P relative to free gas at a temperature T and a pressure of 1 atm (J/kg)

η_d = Dilatational viscosity of hydrogen (Pa-s) = 0 Pa-s in this analysis

κ = Bed permeability (m^2)

μ = Dynamic viscosity of hydrogen (Pa-s)

ρ = Mass density of hydrogen (kg/m^3)

ρ_{Ads} = Bulk mass density of adsorbent (kg/m^3)

$\underline{\underline{\tau}}$ = Fluid stress tensor (Pa)

Abbreviations

DOE = US Department Of Energy

HSECoE = Hydrogen Storage Engineering Center of Excellence

NIST = National Institute of Standards and Technology

SRNL = Savannah River National Laboratory

UQTR = University du Québec à Trois Rivières

1. INTRODUCTION

Hydrogen fueled vehicles can readily compete with traditional liquid hydrocarbon fueled automobiles only if the energy density of the hydrogen stored on board can closely approach or achieve that of liquid fuels. To this end, there are three feasible storage options are available today. Hydrogen can be stored as compressed gas at high pressures, liquefied, or stored by forming chemical or physical bonds with other materials. The first two possibilities require either very high pressure (on the order of 350-700 bar for compressed hydrogen storage) or very low temperatures (on the order of 20-30 K for liquefied hydrogen storage) [1]. High pressure compressed hydrogen storage requires significant compression work and feasible materials that can work at such conditions. Liquid hydrogen storage requires compression work on the order of two to three times the ideal Carnot liquefaction work (3.3 kWh/kg) [2], making the technique particularly expensive. The third storage option, which sees the adoption of materials that bond with hydrogen, is particularly attractive. This concept is characterized by several positive aspects, such as low operating pressures (far lower than for compressed hydrogen storage) and temperatures that are higher than for storage of liquid hydrogen. Metal hydrides and adsorbents are among the most attractive materials to store hydrogen onboard [3,4]. Metal hydrides can achieve relatively good volumetric capacities but, in general, show low gravimetric capacities [5-6] compared to the DOE targets [7]. In addition, many metal hydrides capable of achieving good energy densities suffer from slow kinetics requiring absorption and desorption times longer than the DOE targets of 3-5 min [7]. Alternatively, in materials that adsorb hydrogen by physisorption the hydrogen weight fraction can be noticeably increased and the kinetics become very fast. In

addition, the adsorption process does not involve any phase change in the material, resulting in a high stability after repeated cycling [8]. This gives adsorbents the potential to meet the 2017 DOE targets especially in terms of gravimetric capacity [9-10]. Recently, a class of adsorbents, referred to as Metal Organic Framework (MOF) materials, has been demonstrated and characterized to store hydrogen [11-12]. These materials show higher weight capacities compared to other adsorbent materials, with values of about 2 wt% at room temperature and 20 bar pressure for some modified structures [12]. Several 'ab initio' modeling analyses have been carried out [13,14], as well as experimental synthesis methods have been developed [15,16] to improve the final performance of MOF materials. However, due to the nature of their physical bonds [17-20], hydrogen needs storing at low temperatures (in general on the order of liquid nitrogen temperature) to achieve high H_2 capacities. One of the techniques already investigated to maintain the tank at cryogenic temperatures consists in having a liquid nitrogen bath surrounding the wall of the hydrogen storage tank [9]. An effective approach to adsorb hydrogen at low temperature and reduced time is based on the flow-through cooling concept, which uses low temperature hydrogen fed to the device to maintain the adsorbent material at the required temperature. The technique has been examined and validated from an experimental and modeling point of view showing storage capacities of about 11 wt% (on a material basis for MOF-5®) and reduced charging times [10,21]. The other primary aspect required for an effective storage system is relative to its capacity to effectively desorb the hydrogen and deliver the required hydrogen flow rate under selected operating conditions of pressure and temperature. A new finned heat exchanger concept, based on a honeycomb structure, is proposed for hydrogen desorption in adsorbent storage systems. The concept derives from a similar heat exchanger structure previously used in metal hydride based hydrogen storage systems (namely $NaAlH_4$), which resulted in greatly improved performance compared to plain metal hydride [22]. Honeycomb finned heat exchangers are simple and high volumetric capacity concepts when applied to exchange heat with solid powder systems. These structures are also commercially available at low costs. Application of the honeycomb heat exchanger in adsorbent systems sees the inclusion of a resistive rod heater that provides the required heating power electrically. The paper describes the results obtained within the DOE Hydrogen Storage Engineering Center of Excellence (HSECoE) using the proposed heat exchanger concept in a 0.5 L bench scale adsorbent vessel. The system was demonstrated under different operating conditions from both experimental and modeling points of view, with results reported and discussed in the following sections. The baseline honeycomb system can also easily be optimized and scaled up for large scale vehicular applications.

2. EXPERIMENTAL TEST APPARATUS

Figure 1 shows the UQTR experimental test bench. A 0.5 L flanged tank was used to examine the hydrogen desorption performance adopting a honeycomb finned heat exchanger concept. The device, as shown in Figure 1 a), is comprised of a flanged cylindrical stainless steel tank, with an external diameter of approximately 73 mm and a wall thickness of 5 mm. The length of the tank is about 300 mm. The device is internally insulated using a Teflon® liner structure with an internal diameter of 50 mm and a wall thickness of 6.6 mm. The insulation is required to limit the heat transfer between the internal structure of the tank, which is heated during hydrogen desorption, and the external environment, which is maintained at temperatures on the order of 80 K during the cryogenic temperature tests. A high-level heat transfer calculation was carried out to estimate the required thickness of the liner. Results indicated the need for a Teflon® liner with a thickness of about 6.5 mm, balancing the need for limiting the heat transfer and the need for reduced weight and volume. The weight of the empty structure, including tank, flanges and internal liner, is about 7.2 kg, with the tank representing about 53% of the total weight. Figure 1 b) shows the assembled vessel in horizontal configuration. The honeycomb structure was placed inside the device and filled with MOF-5® adsorbent material. The adsorbent material was acquired from Ford as part of the work carried out within the HSECoE. The material was manually pressed inside each cell of the honeycomb structure applying about the same force, in order to assure approximately the same level of compaction in each cell. Figure 2 shows a schematic of the finned structure filled with adsorbent material and with a single resistive rod heater placed in the central axial position of the honeycomb structure.

Figure 3 shows a more detailed schematic (not to scale) of the glued hexagonal cell structure. The cells are glued together on the horizontal sides of the polygon. The honeycomb structure was acquired from Plascore® with the following geometrical characteristics: (1) cell width (W_c), flat to flat side, equal to 6 mm, (2) cell wall thickness (t_w) equal to 0.1 mm. The nominal power of the electrical heater, required to assure fast hydrogen desorption for the present configuration, was preliminary estimated to be 100 W. Resistive heaters with this level of power are commercially available from Watlow® with diameters on the order of 6 mm, thus matching the size of the selected hexagonal cell.

An important intrinsic characteristic of every commercially available resistive heater is that the temperature distribution along the external surface of the component is not uniform, due to the internal configuration of the resistive rods. Several tests were carried out to identify the temperature distribution on the heater wall, resulting in approximately a parabolic profile. The maximum temperature was achieved approximately at the central axial position, while temperatures did not change at the edges (about 10 mm length) of the heater during the heating

process. The data were collected and suitably included in the numerical model to assure the temperature profiles on the surface were adequately predicted. The vessel, suitably instrumented with thermocouples and pressure transducers, was submerged in liquid nitrogen bath during the cryogenic temperature tests (Figure 4). The volume occupied by the liquid nitrogen bath is several times larger than the vessel volume (Figure 4). The system was designed and built with the intent of maintaining the temperature at the vessel wall as close to liquid nitrogen temperature as possible during the cryogenic temperature tests. The volumetric and gravimetric properties of the overall adsorption system are reported in Table 1.

In addition to the stainless steel vessel, the flanges and the internal Teflon® liner mainly affect the overall system weight and volume. The flanges represent about 32% of the overall system weight without including the honeycomb, heater and adsorbent material. The presence of a Teflon® liner results in a significant decrease of the overall accessible volume, with a reduction of almost 38% of the initial accessible volume (0.94 L). The MOF-5® material occupies about 58% of the initial accessible volume and about 31% of the volume occupied by the overall system, including the vessel wall volume. The weight of the adsorbent material, which was pressed in the cells, reaching a density of about 160 kg/m^3, represents about 1.1% of the overall system weight. The adsorbent material can be compacted further to achieve higher densities, as reported in other studies [9,23,24], but this aspect is beyond the scope of the present work.

3. NUMERICAL MODEL

The system was simulated adopting a detailed transport phenomena model based on mass, momentum and energy balance equations, with additional equations to evaluate the thermodynamic properties of the adsorption system and the gas phase hydrogen.

3.1 Mass, momentum and energy balance equations

The differential equation of the mass balance for hydrogen in gaseous state in the adsorbent porous material is expressed as:

$$\varepsilon \frac{\partial \rho}{\partial t} + \nabla \cdot \left(\rho \vec{v}_s \right) = S_0 \qquad (1)$$

with $\vec{v}_s = \varepsilon \vec{v}$ being the superficial gas velocity and the mass source term being:

$$S_0 = -M_{H2} \rho_{Ads} \frac{\partial n_a}{\partial t} \qquad (2)$$

The mass balance equation of hydrogen flowing in a free volume without porous media and without mass sources is expressed as:

$$\frac{\partial \rho}{\partial t} + \nabla \cdot (\rho \vec{v}) = 0 \tag{3}$$

The differential form of the momentum balance equation (Brinkman equation) for hydrogen flowing inside the porous media under laminar flow conditions is expressed as follows:

$$\begin{aligned} &\frac{\rho}{\varepsilon}\frac{\partial \vec{v}_s}{\partial t} + \left(\frac{\mu}{\kappa} + \frac{S_0}{\varepsilon^2}\right)\vec{v}_s = \\ &-\nabla P + \nabla \cdot \left[\frac{\mu}{\varepsilon}\left(\nabla \vec{v}_s + \nabla \vec{v}_s{}^T\right)\right] - \nabla \cdot \left[\left(\frac{2\mu}{3} - \eta_d\right)\left(\frac{1}{\varepsilon}\right)(\nabla \cdot \vec{v}_s)\underline{\underline{I}}\right] \end{aligned} \tag{4}$$

This equation also includes the viscous stress term expressed in terms of velocity components, taking into account the permeability of the media as well.

For free flows without porous media the momentum balance equation under laminar conditions is expressed as:

$$\rho \frac{D\vec{v}}{Dt} = -\nabla P - \nabla \cdot \underline{\underline{\tau}} \tag{5}$$

adsorbent material and adsorbed hydrogen) and the hydrogen in gaseous state, is expressed as:

$$\begin{aligned} &\varepsilon c \frac{\partial h}{\partial T}\frac{\partial T}{\partial t} - \nabla \cdot k \nabla T \\ &= -c\frac{\partial h}{\partial T}\vec{v}_s \cdot \nabla T \underbrace{- \frac{T}{c}\frac{\partial c}{\partial T}\left(\varepsilon \frac{\partial P}{\partial t} + \vec{v}_s \cdot \nabla P\right)}_{\text{Pressure work}} + \underbrace{\frac{\mu}{\varepsilon}\left[\left(\nabla \vec{v}_s + \nabla^T \vec{v}_s\right) - \left(\frac{2}{3} - \eta_d\right)\nabla \cdot \vec{v}_s \underline{\underline{I}}\right] : \nabla \vec{v}_s}_{\text{Viscous dissipation}} \\ &- \frac{hS_0}{M_{H2}} - \rho_{Ads}\left(\underbrace{\frac{\partial \Delta U_a}{\partial t} + \frac{\partial (u_0 n_a)}{\partial t}}_{\text{Sorption Energy}} + C_{P\ Ads}\frac{\partial T}{\partial t}\right) \end{aligned} \tag{6}$$

Equation 6 is the general energy balance equation in a porous medium reacting with a fluid. It accounts for pressure work term and viscous dissipation term, neglecting terms related to the gravitational potential. The ‘Sorption Energy’ term accounts for the time variation of total internal energy of the adsorbed hydrogen due to the adsorption reaction. To evaluate this term, the numerical model needs to be completed by adding two further relationships assessing ΔU_a.

and n_a. The relative internal energy term (ΔU_a) can be expressed by using the Dubinin-Astakhov (DA) model [17,18]:

$$\Delta U_a = -\frac{n_{\max}\alpha\sqrt{\pi}}{2}\left[1 - erf\left(\sqrt{-\ln\left(\frac{n_a}{n_{\max}}\right)}\right)\right] + n_a\left[RT - \alpha\sqrt{-\ln\left(\frac{n_a}{n_{\max}}\right)}\right] \quad (7)$$

Likewise, the amount of hydrogen adsorbed (n_a) can be evaluated by using the DA model [17,18]:

$$n_a = n_{\max}\exp\left[-\left(\frac{RT}{E_a}\right)^2 \ln^2\left(\frac{P_0}{P}\right)\right] \quad (8)$$

with: $E_a = \alpha + \beta T$

The amount of hydrogen adsorbed (n_a) contributes into the total amount of hydrogen stored inside the bed, as indicated by Equation 9:

$$n_{total} = n_a + c(V_v - V_a) \quad (9)$$

The total amount of hydrogen stored in the bed is given by the hydrogen adsorbed in the material and the hydrogen stored as gas in the void volume at the bulk temperature and pressure.

The bed void fraction value (ε) can be estimated by the following relationship:

$$\varepsilon \equiv \rho_{Ads}(V_v - V_a) \quad (10)$$

For hydrogen flowing into an open volume, the energy balance equation is expressed as follows:

$$c\frac{\partial h}{\partial T}\frac{\partial T}{\partial t} - \nabla\cdot k\nabla T = -c\frac{\partial h}{\partial T}\vec{v}\cdot\nabla T - \frac{T}{c}\frac{\partial c}{\partial T}\left(\frac{\partial P}{\partial t} + \vec{v}\cdot\nabla P\right) - \underline{\underline{\tau}}:\nabla\vec{v} \quad (11)$$

Table 2 shows the DA model parameters for hydrogen adsorption on powder form (non-compacted) MOF-5®. Such values have been assessed at SRNL, in conjunction with Ford, within the HSECoE and validated against experimental data available from Ford [25,10].

The model evaluates the hydrogen state via Equation 12, with the compressibility factor which modifies the ideal gas state equation:

$$P = Z(P,T)\rho RT \quad (12)$$

The compressibility factor was evaluated by the polynomial expression reported in Reference [9]. The hydrogen specific heat, enthalpy, thermal conductivity and viscosity were evaluated by polynomial relationships functions of pressure and temperature, as reported in Reference [9]. The properties of the adsorbent material were evaluated according to Reference [9]. The specific heat was evaluated adopting a cubic spline to interpolate the values of the expression from References [26,10] and included in the model. The expression reported in Reference [26], valid for carbon adsorbents, can be adopted for MOF-5® with limited errors, as demonstrated at conditions close to room temperature [27,10]. The adsorbent material bulk density was assumed equal to 160 kg/m^3, based on the experimental data. The bed thermal conductivity (including adsorbent material and hydrogen) was assumed equal to 0.1 W/mK, based on recent experiments and evaluations carried out within the HSECoE [9,10,27]. The specific heat and thermal conductivity of the material composing the reservoir walls (SS316) and the material of the honeycomb cells (Al6061) were modeled adopting polynomial expressions that fit NIST data [28,29]. The thermal conductivity and the specific heat of Teflon® were estimated using NIST polynomial expressions [30], using a density value of 2200 kg/m^3.

3.2 Model geometry and conditions

The model geometry was set up according to sizes and characteristics of the experimental 0.5 L device available at UQTR. A three dimensional 90° symmetric geometry was adopted to model the actual system. This allows modeling 25% of the overall device structure, resulting in a large reduction of the computing time while still providing an excellent approximation of the actual geometry of the device. A schematic is shown in Figure 5, comprising the following regions: 1) the gas hydrogen region, 2) the honeycomb cell structure with the adsorbent material, 3) the electric heating rod section, 4) the Teflon® liner region, comprised of the top, bottom and circumferential liner structure and 5) the stainless steel walls of the reservoir.

The hydrogen filter was not included in the model, assuming a 100% hydrogen purity without any contaminants. Ten thermocouples were placed inside the experimental reservoir with their positions accounted for in the model geometry as indicated in Figure 6. The first set of thermocouples (TC1, TC4 and TC7) is located at a distance of 8 cm from the upper flange, the second set (TC2, TC5, TC8, TC10) is at a distance of 14.75 cm from the upper flange and the third set (TC3, TC6, TC9) is located at a distance of 22.75 cm from the upper flange. As shown in Figure 6, the thermocouples were placed inside the reservoir with the objective of having them located in the center of each of the three cells composing the honeycomb structure along the radial axis (Y axis of Figure 6). An additional set of cells (TC1, TC2 and TC3) was also placed in contact with the wall of the first cell along the radial axis to monitor the temperature of the cell wall close to the heater.

Mass, momentum and energy conservation equations were integrated by COMSOL Multiphysics® Finite Element software (version 4.2 a), with boundary and initial conditions based on the experimental conditions. Two set of experiments were carried out. The first experiments were performed to evaluate the behavior of the material at room temperature. The initial temperature of the device was equal to 298 K, as measured during the experiments. The heating power ramp was established in agreement with the data recorded during the experiments. The main constraint, limiting the time of application of the maximum power, was given by the maximum allowed adsorbent temperature, required to avoid material damage. This temperature was set to 393 K and the TC2 temperature was the feedback value used to limit the duration of the heating power. Measurements indicated limited temperature gradient at the vessel wall, thus a zero heat flux condition was assumed as wall boundary condition. The initial pressure of the hydrogen stored inside the device was equal to 35 bar, according to the values measured by the pressure transducer during the experiments. The second set of experiments was carried out with the vessel submerged in liquid nitrogen bath. The initial temperature of the device for the cryogenic experiments was set to 84 K, based on the measured data. The heating power ramp used in the numerical simulations was established in agreement with the data recorded during the experiments. A constant temperature (equal to 84 K) value was introduced in the model as boundary condition for the external walls of the device. The temperature was monitored by three thermocouples placed on the external side of the wall device, submerged in liquid nitrogen, which measured a temperature of 84 K throughout the experiments. The initial pressure of the hydrogen stored inside the device was assumed equal to 10 bar, as measured for the hydrogen desorption tests at cryogenic conditions.

4. RESULTS

4.1 Room temperature hydrogen desorption results

Figures 7-9 compare the numerical model results with the corresponding experimental data measured by the 10 thermocouples during room temperature desorption tests. Temperature profiles qualitatively follow the heating power profiles, as shown in Figures 7-9. The model results are in agreement with the experimental data, demonstrating that the model suitably includes and reproduces the main phenomena and properties of the process. The modeling results for the set of thermocouples placed in the upper section of the device (TC1, TC4, TC7) are in excellent agreement with the corresponding experimental data, achieving a maximum difference of about 3 K for the TC7 data, as shown in Figure 7. Figure 8 shows the results obtained for the set of thermocouples placed in the middle of the vessel (TC2, TC5, TC8, TC10), comparing modeling and experimental data. The main differences can be noticed for the TC5 data, with a temperature difference of about 5 K. Figure 9 reports the results obtained for the set of

thermocouples located in the bottom section of the vessel (TC3, TC6, TC9). The main differences between modeling and experimental results are for the TC9 data, with a temperature difference of about 5 K.

Pressure profiles were compared indicating essentially no difference between modeling and experimental data throughout the room temperature experiments. The initial pressure was 35 bar while the maximum pressure achieved in the reservoir (at about 13.5 minutes) was 43 bar.

Table 3 shows the amounts of hydrogen adsorbed and desorbed as calculated by the model. The amount of hydrogen adsorbed (second column of Table 3) was estimated as: $\int_{Vadsorbent} \rho_{Ads} n_a dV$. The amount of free gaseous hydrogen (third column of Table 3) was calculated as: $\int_{Vadsorbent} \rho_{Ads} c(V_V - V_a) dV$. The amount of hydrogen in desorbed state (i.e. gaseous hydrogen) in the honeycomb structure at maximum temperature and pressure (time equal to 13.5 minutes) was about 1.484 g, desorbing about 17% of the hydrogen adsorbed in the material at the beginning of the experiment.

4.2 Cryogenic temperature hydrogen desorption results

Figures 10-12 compare the model results with the corresponding experimental data measured by the 10 thermocouples during cryogenic temperature desorption tests, showing a good agreement. The profiles qualitatively follow the heating power profiles, as shown in Figures 10-12. The model results for the set of thermocouples located in the upper region of the vessel (TC1, TC4, TC7) are in very good agreement with the corresponding experimental data, achieving a maximum difference of about 14 K for TC7 at about 6 minutes, as shown in Figure 10. This difference represents about 14.5% of the overall TC7 temperature variation throughout the low temperature desorption test. The model predicts the maximum temperatures achieved by the set of thermocouples close to the up flange in excellent agreement with the experimental data (about 215 K). Figure 11 shows the results obtained for the set of thermocouples placed in the middle of the vessel (TC2, TC5, TC8, TC10). The main differences are relative to TC10 data, with a maximum temperature difference of about 20 K. However, the experimental data showed remarkable fluctuations during the tests, especially during the last part of the experiments from 12 min to 17 min. Results in Figure 11 show that the model can predict the maximum temperature achieved during the experiments again in excellent agreement with experimental data, showing a difference of about 4 K. Figure 12 reports the results obtained for the set of thermocouples located in the bottom of the vessel (TC3, TC6, TC9). The main differences between modeling and experimental results are relative to TC9 data, with temperature differences of about 10 K.

Likewise the room temperature tests, pressure profiles were compared highlighting basically no difference between modeling and experimental data. The initial measured pressure was 10 bar with the maximum pressure, achieved at about 17 minutes, equal to 57 bar.

Table 4 shows the hydrogen desorption results as calculated by the model. The amounts of hydrogen adsorbed and desorbed shown in Table 4 were estimated as described in the room temperature test section (§ 2.1). The cryogenic conditions allow almost 45% of the initial hydrogen adsorbed in the MOF-5® to be desorbed, with pressure increase of more than 45 bar.

4.3 Hydrogen discharge simulation results

Based on the results obtained from the experimental tests, additional modeling analyses were carried out to predict the behavior of the 0.5 L device during hydrogen discharging under cryogenic conditions. The objective of the simulation was to evaluate the effectiveness of the honeycomb system for hydrogen discharging, especially in terms of time required to discharge the hydrogen required to drive an automotive fuel cell. The 0.5 L reservoir was still assumed to be submerged in liquid nitrogen with the thermal power, required to desorb the hydrogen, provided by an electric heater, working at a nominal power of 100 W. The hydrogen desorbed from the material was allowed to flow from the bottom section of the device. Based on the DOE targets [10], a minimum hydrogen pressure of 5 bar, required for the fuel cell operation, was assumed as boundary condition of the outlet section, throughout the discharging process. The initial conditions of the device were assumed in agreement with the targets and data assumed within the HSECoE and based on the measured values for the current experimental tests. Consequently, the initial hydrogen pressure inside the vessel was assumed to be 100 bar and the initial vessel temperature was assumed to be 84 K. Figure 13 shows the profiles of the heater power and of the pressure applied at the outlet section of the storage system, during a discharging process of about 500 s. Two discharge conditions were assumed and analyzed. The first discharge condition (up to 150 s) saw a constant pressure of 100 bar applied at the outlet section of the device. The heating power was assumed to increase up to the nominal value of about 100 W, in approximately 40 s. The second discharge condition (150 - 500 s) saw the simultaneous application of the heater power at the nominal value of 100W and the reduction of the outlet section pressure to the minimum pressure of 5 bar. The objective was to evaluate the influence of both pressure variation and thermal power as separate contributions (the first discharge condition) and simultaneous contributions (the second discharge condition) on the performance of the system. Figure 14 shows the profiles of the total mass of hydrogen (adsorbed and as free gas) stored in the device (the ‘Inside’ profile in Figure 14) and the mass of hydrogen that exited the device, and driving the fuel cell (the ‘Out’ profile in Figure 14). The amount of hydrogen initially stored in the system (at 84 K and 100 bar) is 23.5 g. The application of an

external heat source (at about 100 W), without any pressure variation, allows about 25% of the hydrogen, previously stored in the device, to be discharged in about 150 s. The simultaneous application of the heating power and reduction of the applied pressure at the outlet section (from 100 bar to 5 bar) results in a significant increase in the hydrogen outlet flow rate. Under these conditions about 12.3 g of hydrogen (52.2% of the hydrogen initially stored in the device) was discharged in about 20 s (Figure 14). This implies that a hydrogen flow rate of about 0.62 g/s can be achieved applying a heating power of about 100 W. The profiles shown in Figure 14 for 170 – 500 s demonstrate that a final asymptotic status can be achieved in less than 500 s, with all the available hydrogen (about 79.3% of the initial hydrogen stored in the device) discharged from the device.

The corresponding temperatures during the discharge transients are shown in Figure 15, which reports the profiles for the three thermocouples (TC5, TC8, TC10) placed in the middle position of the vessel. An initial increase of the adsorbent temperatures is observed while applying heating power, without any pressure variation at the outlet section. Under these conditions a maximum temperature variation of about 53.5 K was achieved at the thermocouple closer to the heater location (TC5). The rapid reduction of the pressure applied at the out section caused a sudden drop in the temperatures, reaching a minimum value of about 66 K inside the vessel (at TC10) at approximately 170 s. In the last part of the discharging process (170 – 500 s) the influence of the heating power became more important than the pressure reduction. The temperatures inside the vessel reached values on the order of 170 -200 K, which resulted in the discharge of the remaining available hydrogen in the device.

5. SUMMARY AND CONCLUSIONS

One of the technical obstacles to make hydrogen adsorbent storage systems viable for use in fuel cell driven automobiles is relative to the ability to desorb hydrogen, matching the fuel cell requirements. Research conducted by the HSECoE verified the potential of a new honeycomb structure heat exchanger to be an effective concept integrated in an adsorbent based hydrogen storage system. The system investigated in the study was filled with MOF-5® adsorbent and the required heating power was provided by a 100 W electric heating element, placed in the center of the honeycomb. A bench scale vessel, with an accessible volume of about 0.5 L, was built, instrumented and tested at UQTR under different operating conditions. Two experimental tests were carried out. The first test aimed to evaluate the behavior of the system during hydrogen desorption at room temperatures. The bench scale system desorbed hydrogen properly. However, only limited temperature variations were permitted at this condition, limiting the maximum temperature of the material to values lower than 393 K to avoid material damage. Thus, only a limited amount of hydrogen initially adsorbed in the material (about 17% of the available

hydrogen) could be desorbed. The second test aimed to evaluate the behavior of the system during cryogenic temperature hydrogen desorption. The bench scale system desorbed about 45% of the initial hydrogen adsorbed in the material. The system was also evaluated and demonstrated from a modeling point of view. After a description of the model adopted, which accounts for mass, energy and momentum balance, the results were presented. The model well replicated the behavior of the system in terms of temperatures, pressures and hydrogen concentrations. The results were in generally good agreement with the experimental data obtained for both the room temperature tests and the cryogenic temperature tests. Additional modeling activities were carried out to evaluate the actual behavior of the bench scale system during hydrogen discharging (i.e. hydrogen flowing out of the device to drive a fuel cell). To model this case, typical realistic operating conditions were assumed with pressure variation between 100 bar and 5 bar during desorption and an adsorption temperature of about 84 K. The same heating power of 100 W was assumed to model this case. The system demonstrated the ability to reach hydrogen discharge flow rates up to about 0.62 g/s under heating power of 100 W. In addition, all the available hydrogen could be discharged in less than 500 s applying 100 W heating power and a pressure reduction from 100 bar to 5 bar. The results obtained for the non-optimized, small scale, storage system investigated in this study demonstrated the potential for the honeycomb as heat exchanger for the purpose of enhancing the rate of hydrogen desorption. Both numerical and experimental investigations will be carried out for larger and optimized storage systems that drive the actual automotive fuel cell system and fully meet the DOE targets for both adsorption and desorption of hydrogen.

ACKNOWLEDGEMENTS

This work was performed as part of the US DOE's Hydrogen Storage Engineering Center of Excellence. The authors gratefully acknowledge the support, insight and assistance by Drs. Ned Stetson and Jesse Adams, who were the DOE managers for this effort.

REFERENCES

1. Gardiner M. Energy requirements for hydrogen gas compression and liquefaction as related to vehicle storage needs. DOE Hydrogen Program Record, Record # 9013, (2009).

2. Syed MT, Sherif SA, Veziroglu TN, Sheffield JW. An economic analysis of three hydrogen liquefaction systems. Int J Hydrogen Energy 1998;23(7):565-576.

3. Hirscher M. Handbook of Hydrogen Storage: New Materials for Future Energy Storage (Wiley, Weinheim, 2010).

4. Broom DP. Hydrogen Storage Materials: The Characterization of Their Storage Properties (Springer, London, 2011).

5. Corgnale C, Hardy BJ, Tamburello DA, Garrison SL, Anton DL. Acceptability envelope for metal hydride-based hydrogen storage systems. Int J Hydrogen Energy 2012;37:2812-24.

6. Pasini JM, Corgnale C, van Hassel B, Motyka T, Kumar S, Simmons K. Metal hydride material requirements for automotive hydrogen storage systems. Int J Hydrogen Energy 2013;38:9755-9765.

7. US DOE Targets for Onboard Hydrogen Storage Systems for Light-Duty Vehicles. Available at https://energy.gov/eere/fuelcells/downloads/doe-targets-onboard-hydrogen-storage-systems-light-duty-vehicles . (Accessed June 2017)

8. Broom DP, Book D. Advances in Hydrogen Production, Storage and Distribution, ed. by A. Basile, A. Iulianelli (Woodhead Publishing, Cambridge, 2014), p. 410.

9. Hardy B, Corgnale C, Chahine R, Richard M-A, Garrison S, Tamburello D, et al. Modeling of adsorbent based hydrogen storage systems. Int J Hydrogen Energy 2012;37:5691-5705.

10. Corgnale C, Hardy B, Chahine R, Cossement D, Tamburello D, Anton D. Simulation of hydrogen adsorption systems adopting the flow through cooling concept. Int J Hydrogen Energy 2014;39(30):17083-91.

11. Li H, Eddaoudi M, O'Keeffe M, Yaghi OM. Design and synthesis of an exceptionally stable and highly porous metal-organic framework. Nature 1999;402:276-279.

12. Rosi NL, Eckert J, Eddaoudi M, Vodak DT, Kim J, O'Keeffe M, et al. Hydrogen storage in microporous metal-organic frameworks. Science 2003;300(5622):1127-1129.

13. Mulder FM, Dingemans TJ, Wagemaker M, Kearley GJ. Modelling of hydrogen adsorption in the metal organic framework MOF5. Chemical Physics 2005;317(2-3):113-118.

14. Sillar K, Hofmann A, Sauer J. Ab Initio Study of Hydrogen Adsorption in MOF-5. Journal of the American Chemical Society 2009;131(11):4143-4150.

15. Kaye SS, Dailly A, Yaghi OM, Long JR. Impact of Preparation and Handling on the Hydrogen Storage Properties of Zn4O(1,4-benzenedicarboxylate)3 (MOF-5). Journal of the American Chemical Society 2007;129(46):14176-14177.

16. Tranchemontagne DJ, Hunt JR, Yaghi OM. Room temperature synthesis of metal-organic frameworks: MOF-5, MOF-74, MOF-177, MOF-199, and IRMOF-0. Tetrahedron 2008;64(36):8553-8557.

17. Richard M-A, Benard P, Chahine R. Gas adsorption process in activated carbon over a wide temperature range above the critical point. Part 1: modified Dubinin-Astakhov model. Adsorption 2009;15:43-51.

18. Richard M-A, Benard P, Chahine R. Gas adsorption process in activated carbon over a wide temperature range above the critical point. Part 2: conservation of mass and energy. Adsorption 2009;15:53-63.

19. Talu O, Myers A. Molecular simulation of adsorption: Gibbs dividing surface and comparison with experiments. AIChE Journal 2001;47(5):1160-1168.

20. Bhatia S, Myers A. Optimum conditions for adsorptive storage. Langmuir 2006;22(4):1688-1700.

21. Tong L, Xiao J, Cai Y, Benard P, Chahine R. Thermal effect and flow-through cooling of an adsorptive hydrogen delivery tank. Int J Hydrogen Energy 2016;41(36):16094-16100.

22. Bhouri M, Goyette J, Hardy BJ, Anton DL. Honeycomb metallic structure for improving heat exchange in hydrogen storage system. Int J Hydrogen Energy 2011;36:6723-6738 .

23. Goldsmith J, Wonf-Foy AG, Cafarella MJ, Siegel DJ. Theoretical Limits of Hydrogen Storage in Metal–Organic Frameworks: Opportunities and Trade-Offs. Chem Mater 2013;25(16):3373-3382.

24. Broom DP, Webb CJ, Hurst KE, Parilla PA, Gennett T, Brown CM, et al. Outlook and challenges for hydrogen storage in nanoporous materials. Applied Physics A 2016;122:151.

25. Sudik A. Personal communications. Ford, 2011.

26. Pyda M, Bartkowiak M, Wunderlich B. Computation of heat capacities of solids using a general Tarasov equation. J Thermal Analysis 2009;52(2):631-656.

27. Ming Y, Purewal J, Liu D, Sudik A, Xu C, Yang J et al. Thermophysical properties of MOF-5 powders. Microporous and Mesoporous Materials 2014;185:235-244.

28. Stainless steel properties. Available at http://cryogenics.nist.gov/MPropsMAY/316Stainless/316Stainless_rev.htm. (Accessed July 2017).

29. Aluminum properties. Available at http://www.cryogenics.nist.gov/MPropsMAY/6061%20Aluminum/6061_T6Aluminum_rev.htm . (Accessed July 2017).

30. Marquardt ED, Le JP, Radebaugh R. Cryogenic material properties database. 11th International Cryocooler Conference, June 20-22, 2000. Available online at http://www.cryogenics.nist.gov/Papers/Cryo_Materials.pdf (Accessed June 2017)

Tables

Table 1: Mass and volume of the main components of the bench scale (0.5 L) adsorbent system

	Mass (kg)	Volume (L)
Empty cylindrical vessel	3.800	0.940* 0.475**
Teflon® liner	0.765	0.356
Honeycomb hexagonal structure	0.039	0.015
Heater	0.036	8.421E-3
Flanges	2.600	0.325
Additional equipment (filter, gaskets, etc)	0.800	0.024
Adsorbent material	0.089	0.545

* Internal volume, ** Volume occupied by the vessel walls

Table 2: Model parameters for MOF-5®

n_{max} [mol/kg of adsorbent]	96.4
P_0 [MPa]	1387
α [J/mol]	2985
β [J/mol K]	15.3
V_a [m^3/(kg of adsorbent)]	0.0017
V_v [m^3/(kg of adsorbent)]	0.00725

Table 3: Hydrogen desorption conditions and states for the room temperature tests

Condition	Hydrogen adsorbed (g)	Free gas hydrogen (g)
Initial state (Time t = 0 min) T = 298 K, P = 35 bar	0.372	1.420
Max temperature state (Time t = 13.5 min) T = variable, P = 43 bar	0.308	1.484

Table 4: Hydrogen desorption conditions and states for the cryogenic temperature tests

Condition	Hydrogen adsorbed (g)	Free gas hydrogen (g)
Initial state (Time t = 0 min) T = 84 K, P = 10 bar	4.372	1.888
Max temperature state (Time t = 17 min) T = variable, P = 57 bar	2.416	3.844

FIGURES

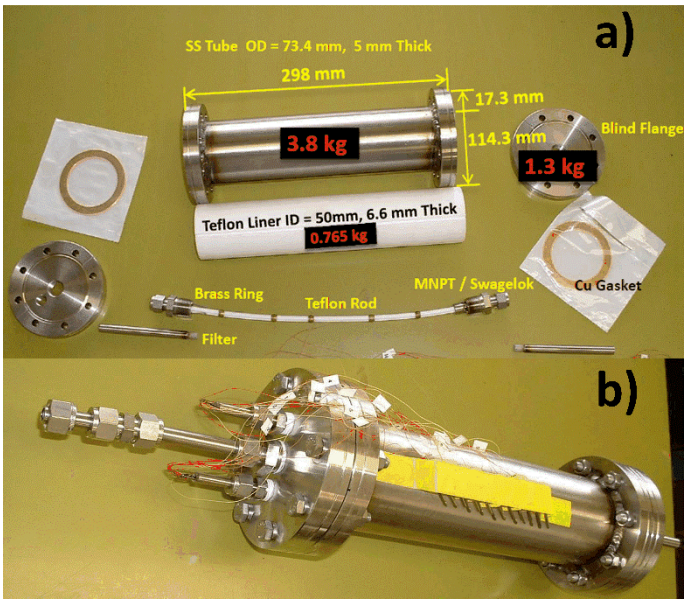

Figure 1: Bench scale vessel: a) components of the 0.5 L vessel; b) assembled vessel in horizontal configuration

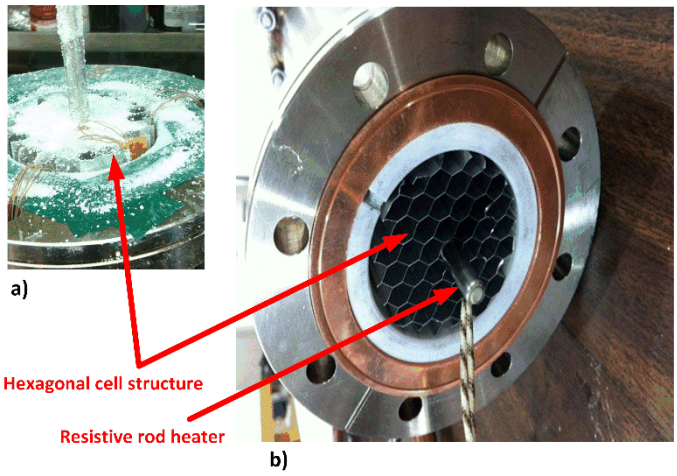

Figure 2: Honeycomb structure with resistive rod heater: a) the hexagonal cell structure is filled with MOF-5® material and placed in the 0.5 L vessel; b) the empty hexagonal cell structure is equipped with the resistive heater placed in the center of the structure

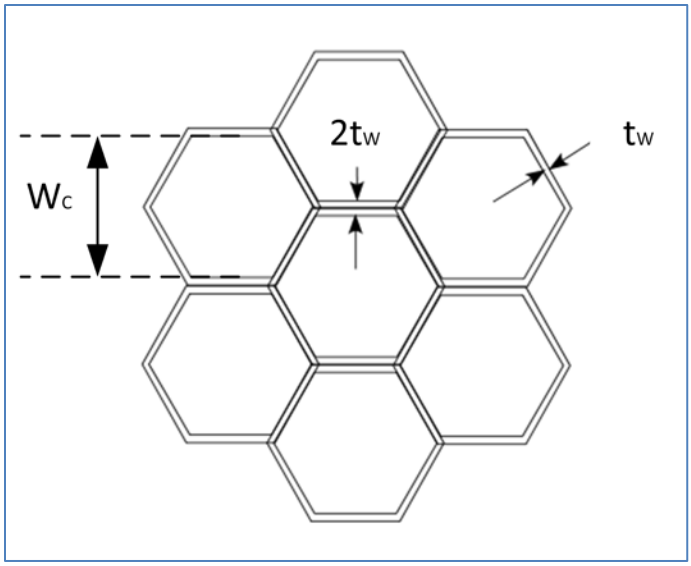

Figure 3: Honeycomb cell structure schematic, with the hexagonal cells glued together on the horizontal sides of the polygon

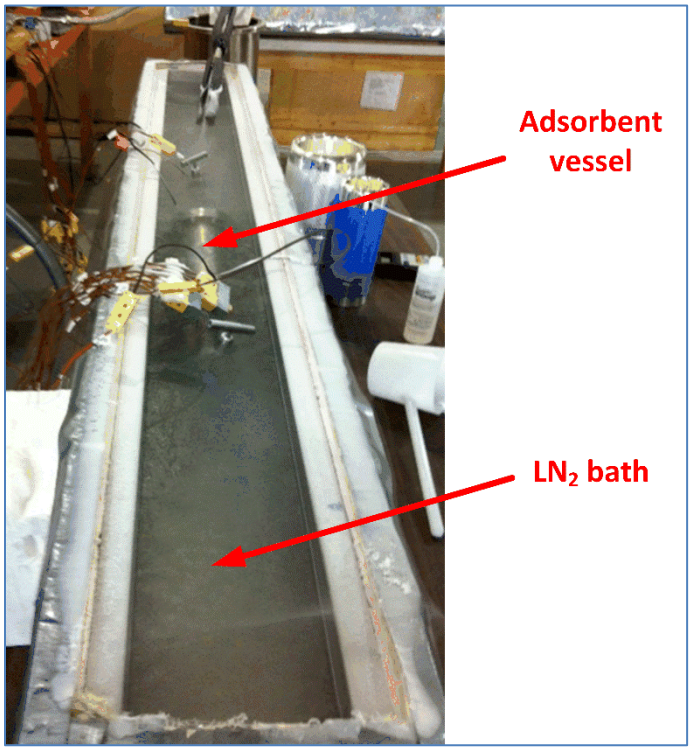

Figure 4: Liquid N_2 bath experimental apparatus

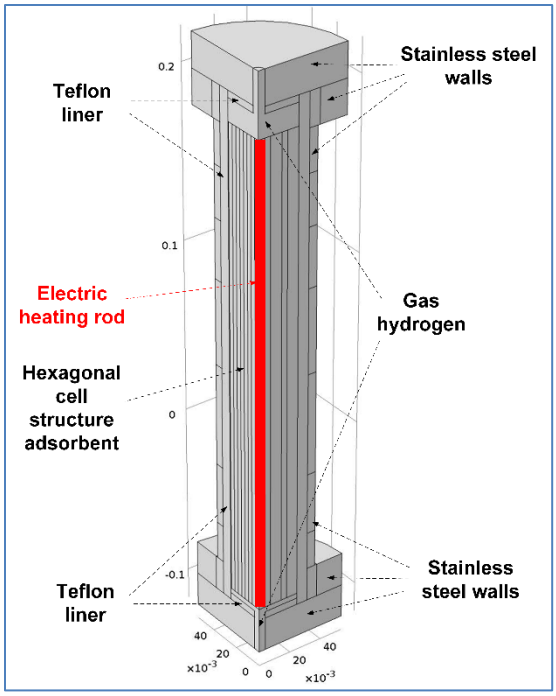

Figure 5: Geometry of the vessel in vertical configuration adopted in the numerical simulations

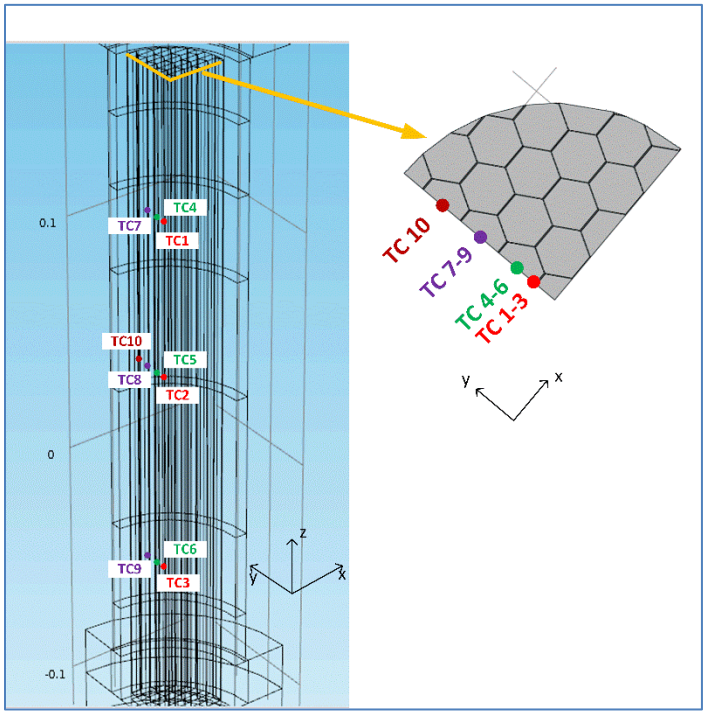

Figure 6: Thermocouple positions in the vertical configuration vessel

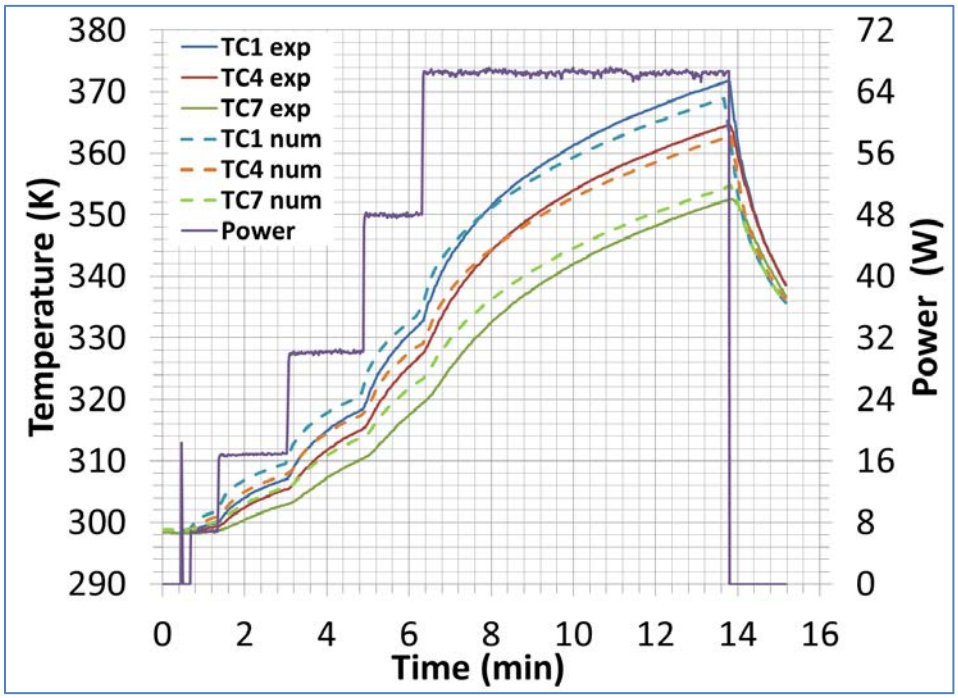

Figure 7: Heating power profile and TC1, TC4 and TC7 temperature profiles (from experiments and numerical model) for the room temperature desorption tests

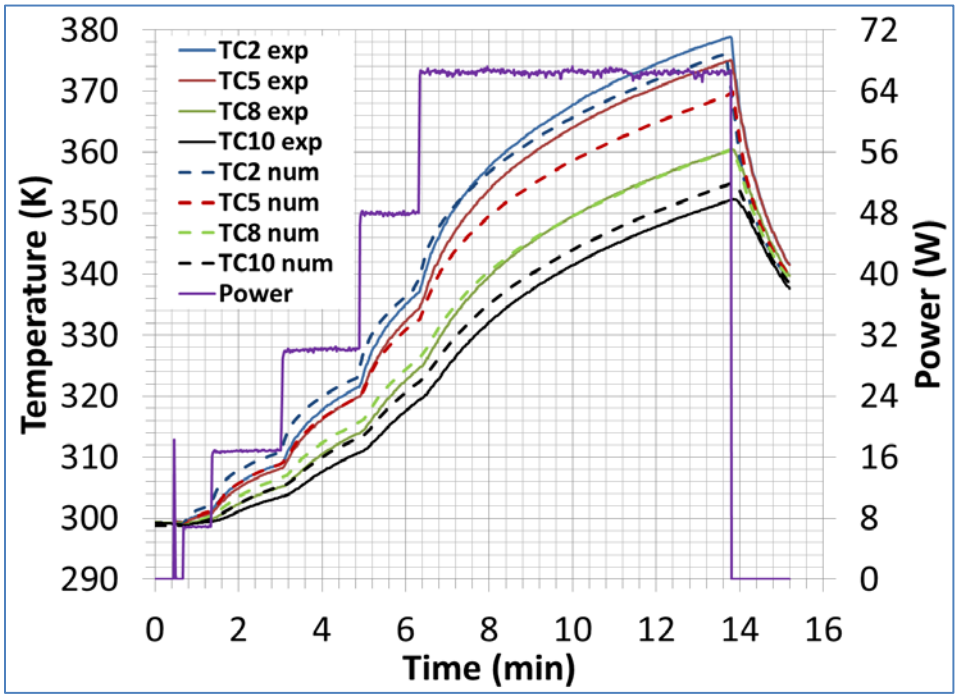

Figure 8: Heating power profile and TC2, TC5, TC8 and TC10 temperature profiles (from experiments and numerical model) for the room temperature desorption tests

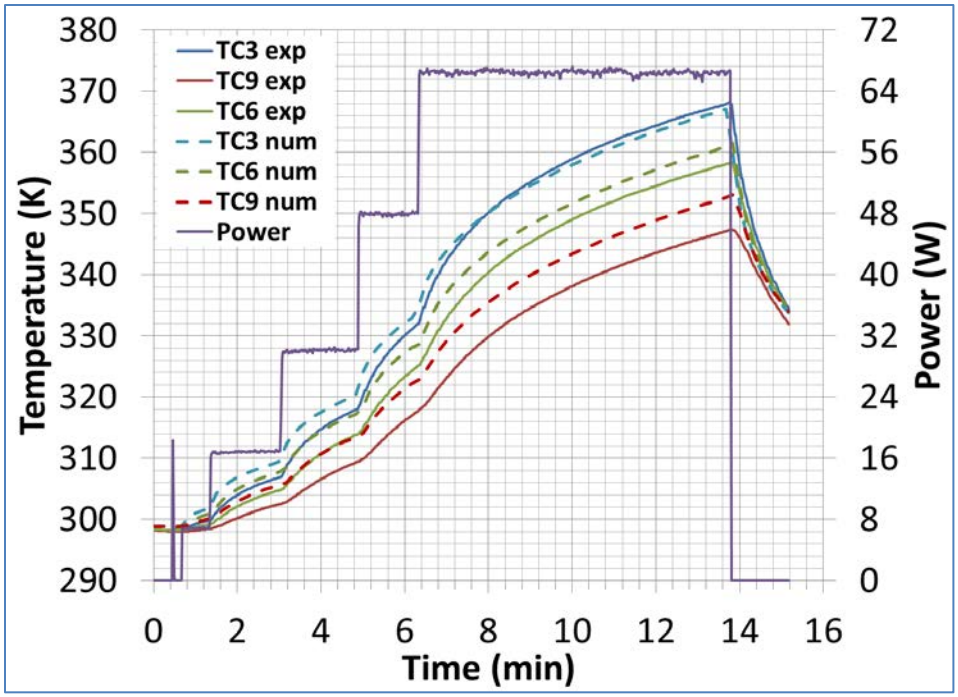

Figure 9: Heating power profile and TC3, TC6 and TC9 temperature profiles (from experiments and numerical model) for the room temperature desorption tests

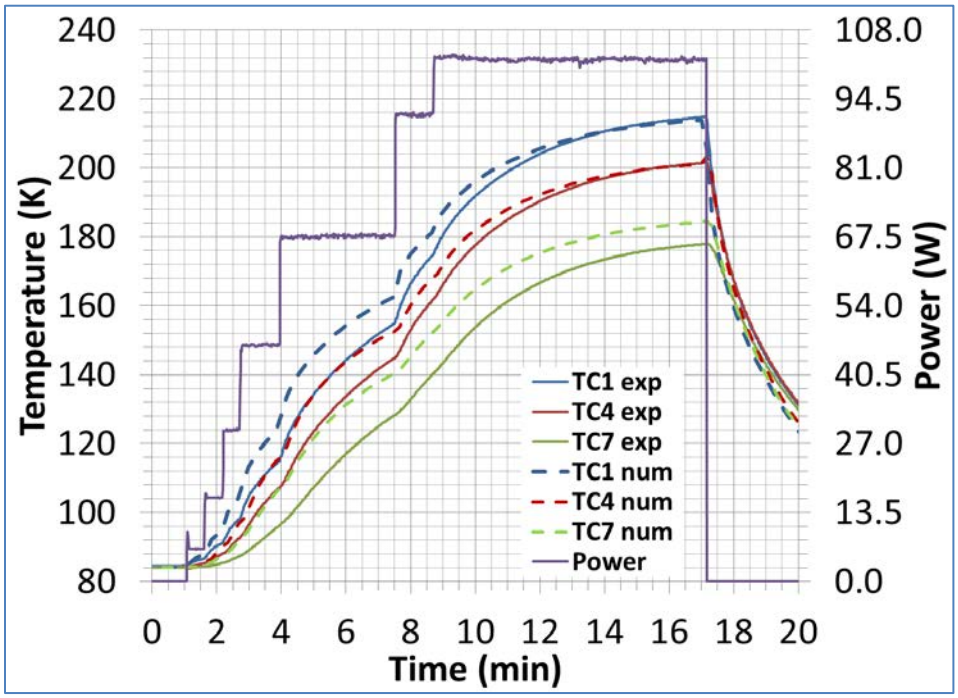

Figure 10: Heating power profile and TC1, TC4 and TC4 temperature profiles (from experiments and numerical model) for the cryogenic temperature desorption tests

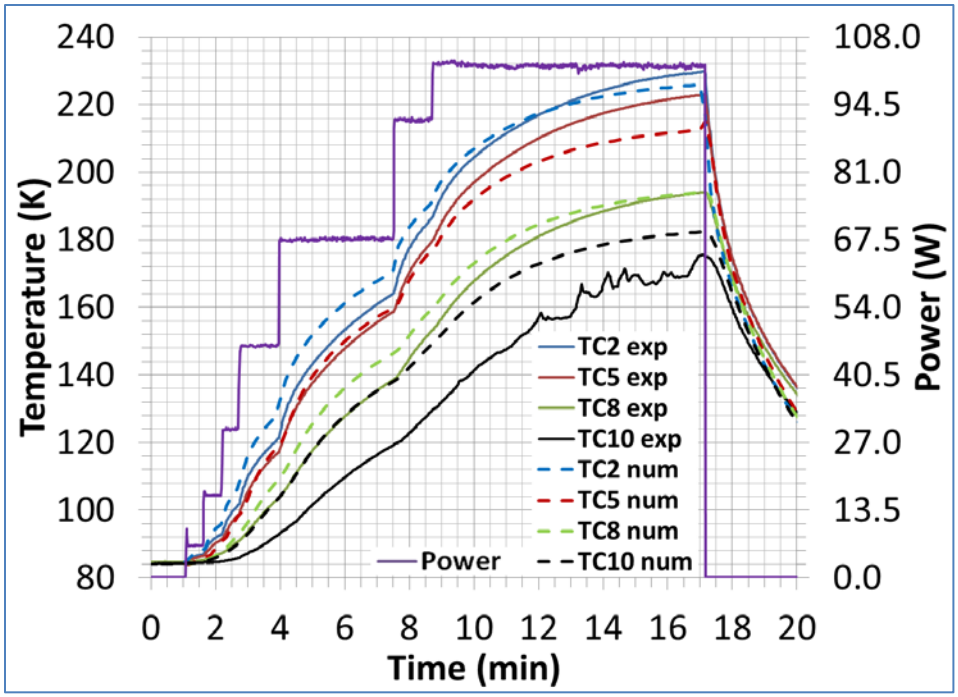

Figure 11: Heating power profile and TC2, TC5, TC8 and TC10 temperature profiles (from experiments and numerical model) for the cryogenic temperature desorption tests

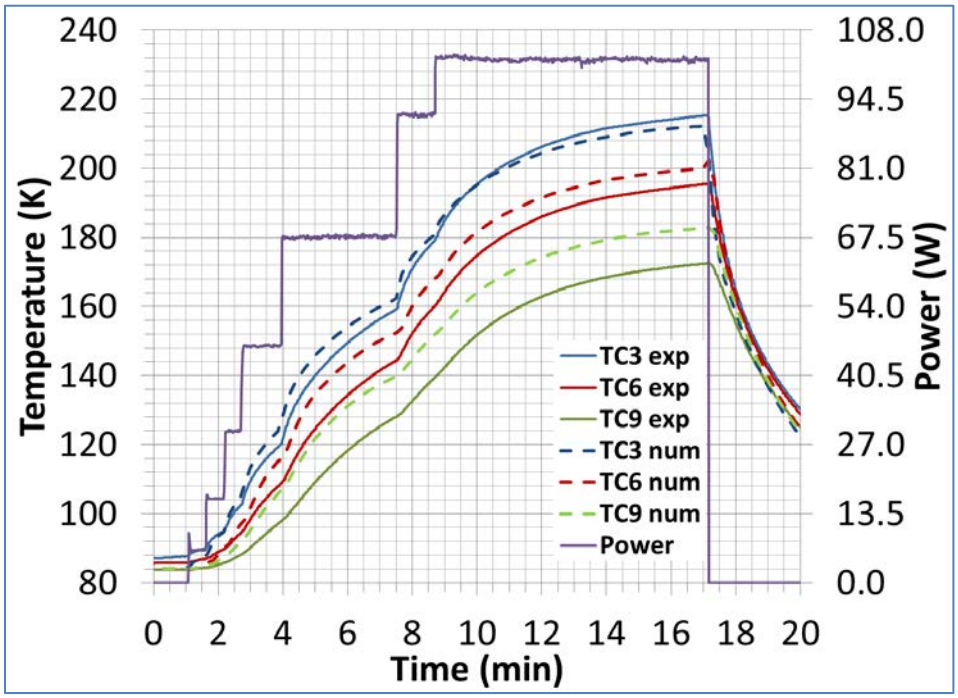

Figure 12: Heating power profile and TC3, TC6 and TC9 temperature profiles (from experiments and numerical model) for the cryogenic temperature desorption tests

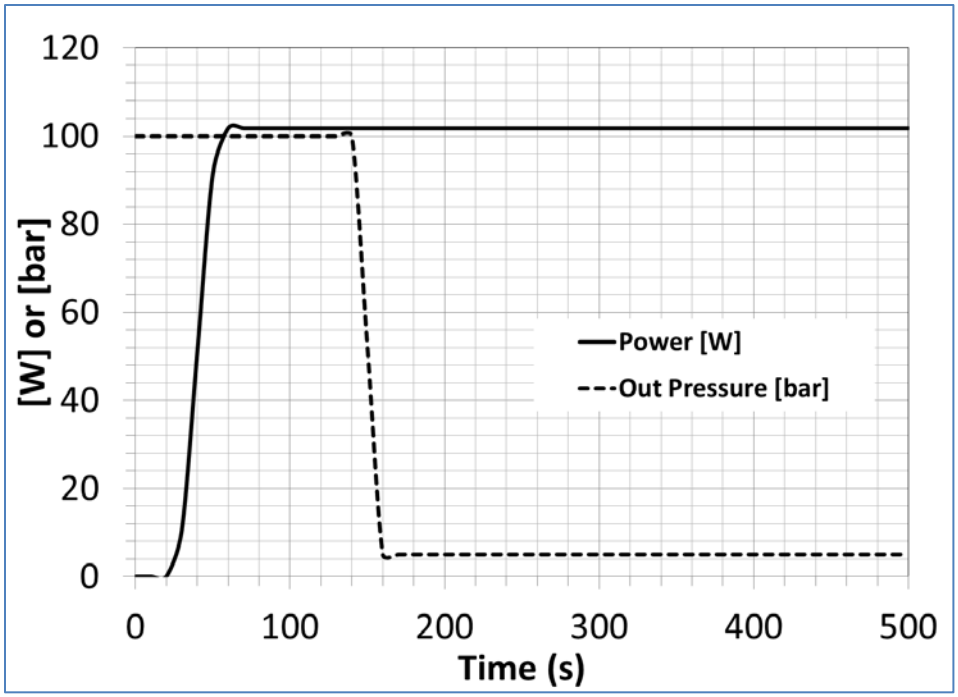

Figure 13: Heating power and applied outlet section pressure modeling profiles for the cryogenic temperature hydrogen discharging tests

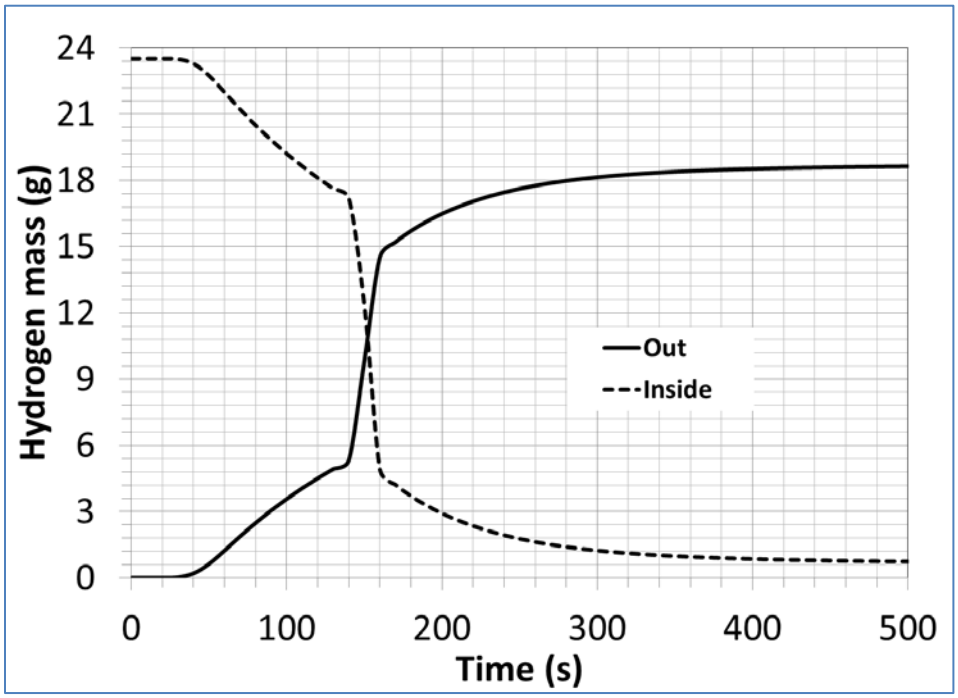

Figure 14: Modeling profiles of the hydrogen mass present inside the vessel at a given instant in time (‘Inside’) and the mass of hydrogen that flowed out of the device up to a given time (‘Out’) for the cryogenic temperature hydrogen discharging tests

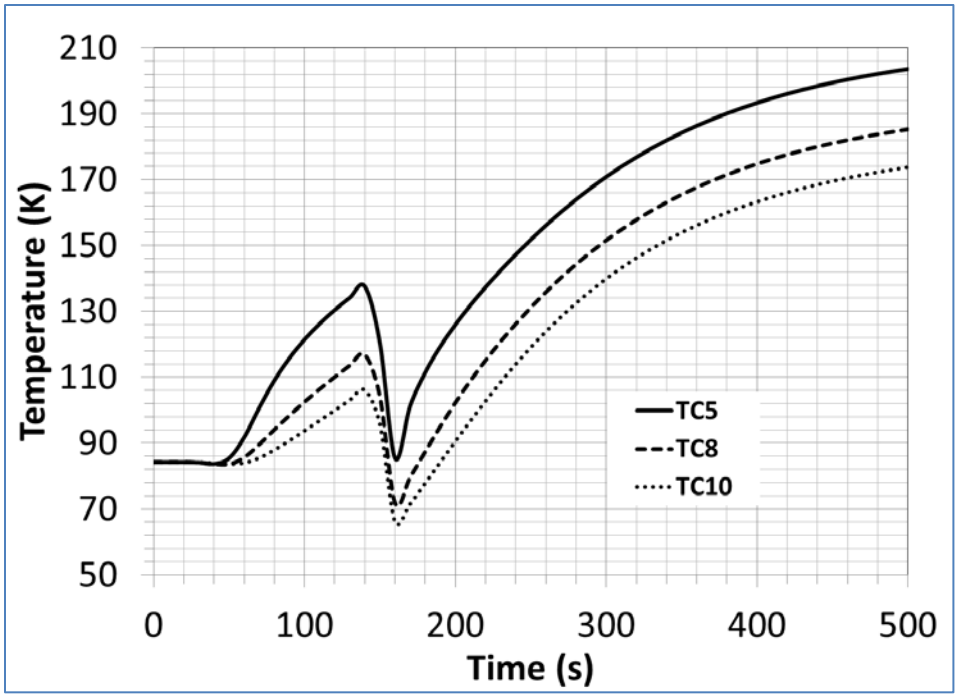

Figure 15: TC5, TC8 and TC10 temperature modeling profiles for the cryogenic temperature hydrogen discharging tests